ORIGINAL ARTICLE

KCTD4 interacts with CLIC1 to disrupt calcium homeostasis and promote metastasis in esophageal cancer

Cancan Zheng[a,†], Xiaomei Yu[a,†], Taoyang Xu[a,†], Zhichao Liu[b], Zhili Jiang[c], Jiaojiao Xu[a], Jing Yang[a], Guogeng Zhang[a], Yan He[a], Han Yang[d], Xingyuan Shi[c], Zhigang Li[b], Jinbao Liu[e], Wen Wen Xu[e,*]

[a]Key Laboratory of Biological Targeting Diagnosis, Therapy and Rehabilitation of Guangdong Higher Education Institutes, the Fifth Affiliated Hospital of Guangzhou Medical University, Guangzhou 510230, China
[b]Department of Thoracic Surgery, Shanghai Chest Hospital, School of Medicine, Shanghai Jiao Tong University, Shanghai 200030, China
[c]Department of Radiation Oncology, the Fifth Affiliated Hospital of Guangzhou Medical University, Guangzhou 510230, China
[d]Department of Thoracic Surgery, Sun Yat-sen University Cancer Center, Guangzhou 510060, China
[e]Guangdong Provincial Key Laboratory of Protein Modification and Degradation, State Key Laboratory of Respiratory Disease, and School of Basic Medical Sciences, Guangzhou Medical University, Guangzhou 511495, China

Abstract   Increasing evidences suggest the important role of calcium homeostasis in hallmarks of cancer, but its function and regulatory network in metastasis remain unclear. A comprehensive investigation of key regulators in cancer metastasis is urgently needed. Transcriptome sequencing (RNA-seq) of primary esophageal squamous cell carcinoma (ESCC) and matched metastatic tissues and a series of gain/loss-of-function experiments identified potassium channel tetramerization domain containing 4 (KCTD4) as a driver of cancer metastasis. KCTD4 expression was found upregulated in metastatic ESCC. High KCTD4 expression is associated with poor prognosis in patients with ESCC and contributes to cancer metastasis *in vitro* and *in vivo*. Mechanistically, KCTD4 binds to CLIC1 and disrupts its dimerization, thus increasing intracellular Ca^{2+} level to enhance NFATc1-dependent fibronectin transcription. KCTD4-induced fibronectin secretion activates fibroblasts in a paracrine manner, which in turn promotes

cancer cell invasion *via* MMP24 signaling as positive feedback. Furthermore, a lead compound K279-0738 significantly suppresses cancer metastasis by targeting the KCTD4−CLIC1 interaction, providing a potential therapeutic strategy. Taken together, our study not only uncovers KCTD4 as a regulator of calcium homeostasis, but also reveals KCTD4/CLIC1-Ca^{2+}-NFATc1-fibronectin signaling as a novel mechanism of cancer metastasis. These findings validate KCTD4 as a potential prognostic biomarker and therapeutic target for ESCC.

1. Introduction

Metastasis remains the primary threat to life in cancer patients[1,2]. Tumor metastasis is generally considered a complex and multistep process, with ion channels/transporters participating in each step of the cascade[3]. Recently, the importance of calcium ion (Ca^{2+}) homeostasis in regulating key hallmarks of cancer, such as proliferation and apoptosis, has been gaining increasing recognition. Many signal cascades can be activated by an increase in Ca^{2+} influx; for example, the nuclear factor of activated T cells (NFAT) can translocate into the nucleus to function as a transcription factor[4]. However, the function and regulatory network of Ca^{2+} flux and Ca^{2+}-dependent signaling in tumor metastasis remain largely unknown.

In the present study, we performed transcriptome sequencing (RNA-seq) to compare gene profiles between esophageal squamous cell carcinoma (ESCC) tumor tissues and matched metastatic tissues, as well as between the highly metastatic cell sublines that we established previously and the corresponding parental cells[2]. By overlapping the differentially expressed genes identified in the two cohorts, we selected the potassium channel tetramerization domain containing 4 (KCTD4) as the focus of this study because of its abnormal expression in both metastatic cells and tissues. KCTD4 belongs to the human potassium (K^+) channel tetramerization domain (KCTD) family and contains a conserved N-terminal domain with a common Bric-a-brac, Tramtrack and Broad complex (BTB) domain that is essential for the oligomerization and diverse functions of KCTD family proteins[5,6]. The role of KCTD4 in cancer and the mechanisms involved have not yet been reported. Here, our RNA-seq and Gene Ontology (GO) analyses suggested that Ca^{2+} signaling may account for the biological function of KCTD4. Immunoprecipitation coupled with mass spectrometry (IP−MS) identified chloride intracellular channel 1 (CLIC1) as an interacting protein of KCTD4. CLIC1 forms a dimer to support chloride ion (Cl^-) channel bioactivity[7], but whether CLIL1 mediates the role of KCTD4 in cancer metastasis remains to be elucidated.

In addition to being influenced by genetic/epigenetic changes in tumor cells, tumor metastasis is also influenced by the tumor microenvironment (TME)[8]. As one of the most abundant cell types in the TME, fibroblasts were first defined as cells in connective tissue that synthesize collagen and remain quiescent with limited metabolic and transcriptomic activity[9]. Fibroblasts can be activated to become cancer-associated fibroblasts (CAFs) by appropriate stimulation and contribute to cancer progression by releasing growth factors and cytokines[10]. Revealing the mechanisms by which KCTD4-Ca^{2+} signaling affects cell−cell crosstalk in the TME would be helpful for the development of more precision therapeutic strategies.

In this study, we sought to investigate the biological and clinical significance of KCTD4 in cancer metastasis. The potential implication of small molecules targeting the KCTD4−CLIC1 interaction to suppress tumor metastasis was also evaluated *in vitro* and *in vivo*.

2. Materials and methods

2.1. Cell lines and drugs

The human ESCC cell lines KYSE150, KYSE270, and KYSE410 were purchased from DSMZ (Braunschweig, Germany). The highly metastatic cell line KYSE150-Luc-LM3 was previously established by our laboratory[11,12]. Fibroblasts were isolated from fresh specimens of primary ESCC tumors by a process as previously described[13]. All cell lines were cultured in RPMI 1640 medium (Thermo Fisher Scientific, Waltham, MA, USA) or Dulbecco's Modified Eagle's Medium (DMEM) (Thermo Fisher Scientific) supplemented with 10% fetal bovine serum (FBS) (ExCell Bio, Shanghai, China) and 1% penicillin/streptomycin (Thermo Fisher Scientific) at 37 °C in a 5% CO_2 incubator. BAPTA acetoxymethyl ester (BAPTA-AM) was obtained from Sigma−Aldrich (St. Louis, MO, USA), triptycene-1,4-quinone (INCA-6) was purchased from R&D Systems (Minneapolis, MN, USA), and amlodipine was obtained from Selleck Chemicals (Houston, TX, USA).

2.2. RNA-seq

RNA-seq of KCTD4-overexpressing cells and control cells was performed at Beijing Genomics Institute Tech (Shenzhen, China). Genes with an expression fold change of >2 and a *P* value of <0.05 were defined as differentially expressed genes.

2.3. Transfection and infection

The siRNA and shRNA constructs targeting KCTD4 were obtained from TranSheep Bio (Shanghai, China), and the sequences are listed in Supporting Information Table S1. The coding sequences of human KCTD4 and CLIC1 were inserted into pcDNA3.1 (TranSheep Bio). For the establishment of stable cell lines, the lentiviral packaging plasmids pMDLg/pRRE (Addgene #12251) and pRSV-Rev (Addgene #12253) and the envelope plasmid pMD2.G (Addgene #12259) were co-transfected with the gene overexpression or knockdown plasmids into HEK 293T cells

using Lipofectamine 3000 (Thermo Fisher Scientific) for lentivirus production. The lentivirus-containing supernatants were collected and used for infection of cancer cells before puromycin selection.

2.4. CRISPR/Cas9-mediated genome editing

CLIC1 knockout cells were generated by using a CRISPR/Cas9 approach similar to that previously reported[14]. The single-guide RNA (sgRNA) targeting CLIC1 was obtained from Transheep Bio, and the sequence was as follows: sgCLIC1, GACTCACTGTCATTGAGTGC.

2.5. Tissue microarrays (TMAs) and immunohistochemistry

ESCC TMAs containing 180 tumor samples and 158 matched normal adjacent tissue samples (Shanghai Outdo Biotech, Shanghai, China), as well as 40 pairs of primary tumor and matched metastatic tissues (Biomax, Rockville, MD, USA), were used to analyze the level of KCTD4. After deparaffinization, rehydration, antigen retrieval, and blocking, the slides were incubated at 4 °C overnight with an antibody specific for KCTD4 (Thermo Fisher Scientific). After secondary antibody incubation for 1 h, the sections were stained with 3,3′-diaminobenzidine (DAB) substrate. The staining intensity was categorized into four groups: score 0 (negative), score 1 (weakly positive), score 2 (moderately positive), and score 3 (strongly positive). Samples with scores of 0−1 were considered to have low expression, while those with scores of 2−3 were considered to have high expression.

2.6. Western blot analysis

Western blot analysis was performed as described previously[15]. After blocking with 5% milk for 1 h, PVDF membranes were incubated first with primary antibodies and then with secondary antibodies. The sources and dilutions of the primary antibodies were as follows: anti-KCTD4 (1:1000, Thermo Fisher Scientific), anti-Fibronectin (1:1000, Proteintech, Chicago, IL, USA), anti-E-cadherin (1:5000, BD Biosciences, Bedford, MA, USA), anti-Actin (1;2000, Santa Cruz, Biotechnology, CA, USA), anti-NFATc1 (1:1000, Proteintech), anti-Lamin B (1:1000, Proteintech), and anti-GAPDH (1:1000, Proteintech).

2.7. Cell invasion and migration assays

Invasion and migration assays were performed in 24-well BioCoat Matrigel Invasion Chambers (Corning Co., New York, USA) as previously described[16,17].

2.8. Immunofluorescence and confocal microscopy

Immunofluorescence staining was performed as described previously[18,19]. After culturing for 24 h, cells were washed with precooled phosphate-buffered saline (PBS) and fixed with 4% paraformaldehyde for 15 min at room temperature. Then, the cells were permeabilized with 0.1% Triton X-100 in PBS for 10 min and blocked with 5% bovine serum albumin (BSA) for 1 h. Subsequently, the cells were incubated first with primary antibodies and then with secondary antibodies. Then, 4,6-diamidino-2-phenylindole (DAPI) and phalloidin were used separately to counterstain nuclei and F-actin, respectively. Images were acquired using a confocal microscope.

2.9. Real-time polymerase chain reaction (RT-PCR)

Total RNA from ESCC cells was isolated and purified using a HiPure Total RNA Mini Kit (Guangzhou Magen Biotechnology Co., Ltd., Guangzhou, China) according to the manufacturer's instructions. The concentration of RNA was measured by a spectrophotometer (NanoDrop Technologies Inc., Wilmington, DE, USA). Equivalent quantities of total RNA were used for reverse transcription with the PrimeScript RT Reagent Kit (TaKaRa, Kyoto, Japan). The RT−qPCR primer sequences are listed in Supporting Information Table S2.

2.10. Chromatin immunoprecipitation (ChIP)-quantitative PCR

The ChIP assay was performed using the SimpleChIP Enzymatic Chromatin IP Kit (Cell Signaling Technology) by a process similar to that previously reported[20]. In brief, collected cells were treated sequentially with formaldehyde and ultrasonication for crosslinking and chromatin fragmentation, respectively. Then, an anti-NFATc1 antibody (Abcam, Cambridge, MA, USA) or IgG (Santa Cruz Biotechnology) was added to the fragmented chromatin solution for immunoprecipitation overnight. Chromatin-protein-antibody complexes were obtained after incubation with protein G agarose beads for 2 h at 4 °C, and ChIP DNA fragments were purified with elution buffer and then analyzed by qPCR. The primers used for ChIP are listed in Table S2.

2.11. Co-immunoprecipitation (Co-IP)

Co-IP was performed as previously described[14]. Collected cells were lysed with RIPA buffer to extract the total protein. The cell supernatants were mixed with IgG (Santa Cruz Biotechnology) and protein A/G Sepharose beads (Invitrogen, Gaithersburg, MD, USA) to reduce the disruption of the complex background. After washing, the protein samples were divided into two groups and incubated with a specific primary antibody or IgG overnight. Proteins immunoprecipitated by protein A/G Sepharose beads were analyzed by Western blotting.

2.12. Mass spectrometry (MS)

Protein digestion and MS analysis were performed as previously described. In brief, total protein was extracted from ESCC cells, and the appropriate primary antibody and protein A/G agarose beads were applied to prepare the MS samples. Proteins were digested with trypsin, vacuum-freeze-dried, and desalted with a MonoTIPTM C18 Pipette Tip (GL Sciences, Tokyo, Japan). Peptide samples were analyzed with an Orbitrap Fusion Lumos mass spectrometer (Thermo Fisher Scientific). Proteome Discoverer (Thermo Fisher Scientific) and Spectronaut (Omicsolution Co., Ltd., Shanghai, China) software were used to analyze the raw data.

2.13. Luciferase reporter assay and site-directed mutagenesis

The binding sites of NFATc1 in the fibronectin promoter region were predicted by using JASPAR, and the sequences of the wild-type fibronectin promoter and four mutants were amplified by PCR and subcloned into the PGL3-Enhancer luciferase reporter plasmid (TranSheep Bio). ESCC cells were cotransfected with the wild-type fibronectin promoter or mutant constructs and the NFATc1 expression plasmid or control vector (Promega, Madison,

WA, USA), while a Renilla luciferase expression plasmid was used to evaluate the firefly luciferase intensity. After 48 h of transfection, the relative luciferase activity was measured by the Dual-Luciferase Reporter Assay System (Promega). The mutations were generated by PCR amplification, and the primers are listed in Supporting Information Table S3.

2.14. Label-based (L-Series) human antibody array analysis

A label-based (L-Series) human antibody array (RayBiotech, Norcross, GA, USA) was used to detect cytokines in cell culture supernatants. In brief, the primary amine groups of the proteins in the sample were biotinylated. After blocking, glass slide arrays preprinted with capture antibodies were incubated with the biotin-labeled samples. A streptavidin-conjugated fluorescent dye (Cy3 equivalent) was then applied to the array, and signals were visualized by laser fluorescence scanning.

2.15. Enzyme-linked immunosorbent assay (ELISA)

The concentrations of fibronectin in conditioned medium (CM) were determined with human fibronectin ELISA kits according to the manufacturer's instructions (Thermo Fisher Scientific).

2.16. Purification of KCTD4-GST and CLIC1-His fusion proteins

Protein purification was performed as described previously[21]. The KCTD4 and CLIC1 gene sequences were inserted into the pGEX-4T-1 vector containing a glutathione S-transferase (GST)-flag tag and pET-28b vector containing a His tag, respectively. The KCTD4 and CLIC1 expression plasmids were transformed into E. coli BL21 Star (DE3) cells. The GST-tagged KCTD4 fusion protein and the His-tagged CLIC1 fusion protein were isolated with a GST-tag protein purification kit and a His-tag protein purification kit (both from Beyotime) according to the manufacturer's instructions.

2.17. Molecular docking and compound screening

For protein preparation, the crystallographic structure of the CLIC1 protein was obtained from the PDB website (PDB code 1K0O) and the KCTD4 was predicted by AlphaFold (AF-Q8WVF5-F1). The dockings were carried out in 5400 poses, screened out into 2000 better poses calculated by the ZRANK rescoring method. RMSD values within 2.0 Å were acceptable for the molecular docking-based virtual screening. The pose with the lowest energy of binding was extracted for further analysis according to the MM-PBSA method. "The residues of CLIC1: Glu102, LYS138, ARG208 and the residues of CLIC1: LYS17, ASP72, ASP74, predicted to be the main basic amino acids."

For compound screening, the residues of CLIC1: GLU102, LYS138, ARG208 and the residues of CLIC1: LYS17, ASP72, ASP74 were used as active cavities to screen for inhibitors (center_x = 0.306183, center_y = 3.936521, center_z = 12.079296; Radius = 18.755915). Two molecular docking methods, LibDock and CDOCKER in DS software, were performed in this study. We identified 1,518,105 specific small molecule compounds from a compound library of Chemdiv and Maybridge. Based on the Lipinski Rule of Five and Veber Rule, the 1,146,739 compounds were selected for docking via LibDock

(Number of hotspots = 100, Docking tolerance = 0.25 Å and the docking preference was high quality). Then, the top 2000 small molecules were selected for docking via CDOCKER with standard configuration. Finally, the top 30 compounds with the lowest energy based on the energy score were obtained.

2.18. Super ELISA

Experiments were performed as previously described[22]. In brief, 96-well plates were coated with an anti-GST-tag antibody (Proteintech) by incubation overnight at 4 °C. After washing with PBS, 5% BSA was used for blocking. The purified KCTD4-GST (1 μg) and CLIC1-His fusion proteins were added and incubated at room temperature for 5 and 3 h, respectively. Then, each of the 30 small molecule inhibitors (10 μmol/L) was individually added to each well. After sequential incubation with the anti-His-tag antibody, the corresponding secondary antibody, and tetramethylbenzidine (TMB), the absorbance was measured at wavelengths of 450 and 630 nm.

2.19. Native polyacrylamide gel electrophoresis (PAGE)

Native PAGE was performed using a Native PAGE Preparation Kit (Sangon Biotech, Shanghai, China) according to the manufacturer's instructions. In brief, ESCC cells were lysed to extract native protein samples, and the cell supernatants were then loaded (approximately 20 μg per lane) on in-house-formulated gradient gels. After electrophoresis, native proteins in the gels were transferred to a PVDF membrane and incubated with the appropriate primary antibody and secondary antibody.

2.20. Calcium and chlorine imaging

Calcium imaging was performed to visualize the dynamic changes in Ca^{2+} in the cytoplasm. ESCC cells were incubated in culture medium containing Fluo-4 AM (Thermo Fisher Scientific) for 1 h at 37 °C and subsequently rinsed with PBS. Cells were excited with a low-intensity 488-nm laser, and images were acquired at 1−2 s intervals in time-lapse mode for 10 min. Image data were subsequently analyzed using ImageJ (National Institutes of Health, Bethesda, USA) and the final values are presented as the ratio of F/F0, where F0 is the baseline fluorescence intensity in each cell.

2.21. Measurement of intracellular chloride ion concentration

N-[Ethoxycarbonylmethyl]-6-methoxy-quinolinium bromide (MQAE, Beyotime, Shanghai, China) was used to measure the intracellular chloride ion concentration ($[Cl^-]i$) according to the manufacturer's instructions. In brief, cells were incubated for 45 min in Krebs-HEPES buffer (Beyotime) containing 8 mmol/L MQAE. Then, the cells were washed with Krebs-HEPES buffer 5 times. The corresponding fluorescence was measured with a multimode microplate reader (Varioskan Lux Reader, Thermo Fisher Scientific).

2.22. Lymph node metastasis mouse model

Mice were inoculated subcutaneously in the left hind footpad with 1×10^6 KCTD4-overexpressing or KCTD4-knockout cells. Tumors removed from the region between the footpad region and the
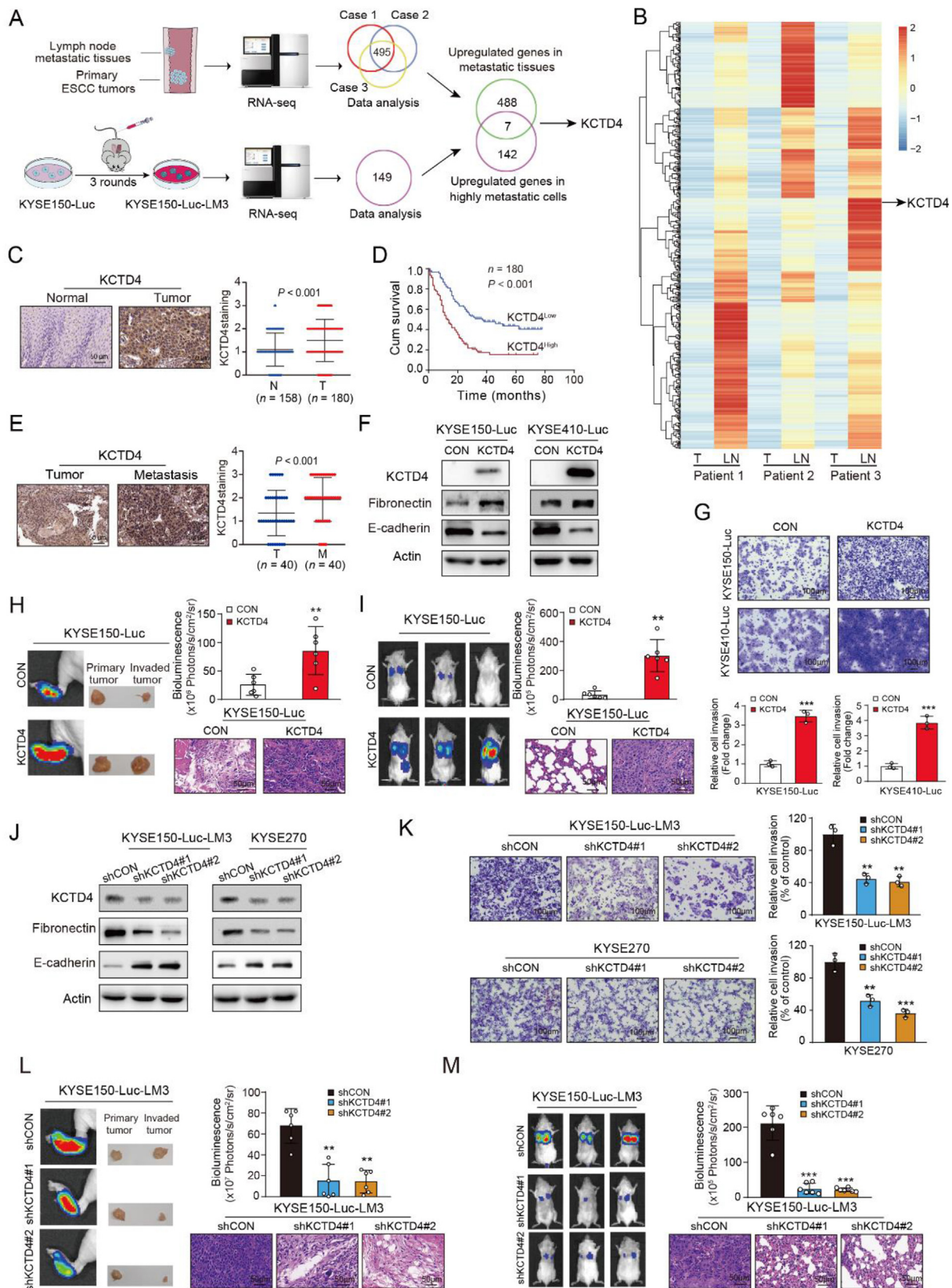
Figure 1 KCTD4 is upregulated in metastatic tissues and contributes to cancer metastasis. (A) Schematics showing the process for screening key regulators contributing to cancer metastasis. Venn diagram showing the approach for investigating the overlapping genes upregulated in metastatic cells and tissues. (B) Heatmap demonstrating the differentially expressed genes between primary ESCC tumors and metastatic tissues. (C) Representative images and pattern of KCTD4 expression in tissue arrays consisting of 180 primary ESCC and 158 matched normal tissues.

Table 1 Correlation between KCTD4 expression levels and clinicopathological parameters in 180 cases of esophageal squamous cell carcinoma.

Variable	n	Low KCTD4	High KCTD4	P value
Age (years)				
≤55	24	11	13	0.62
>55	156	80	76	
Gender				
Female	148	74	74	0.75
Male	32	17	15	
T-Stage				
1/2	32	20	12	0.14
3/4	148	71	77	
N-Stage				
N0	78	49	29	0.004**
N1/N2/N3	102	42	60	
M-Stage				
M0	177	91	86	0.03*
M1	3	0	3	
Grade				
I & II	138	67	71	0.33
III & IV	42	24	18	

*$P < 0.05$; **$P < 0.01$.

ankle joint were considered invaded tumors. Mice were imaged using an IVIS 100 Imaging System (Caliper Life Sciences, Waltham, MA, USA) after intraperitoneal injection of D-luciferin (150 mg/kg in PBS) under anesthesia for exposure. The tumors were resected and fixed with 10% formaldehyde/PBS for histological analysis.

2.23. Experimental metastasis model

The experiment was performed as previously described[13]. In brief, 1×10^6 cells were injected intravenously into mice *via* the tail vein. After 4 weeks, the mice were injected with D-luciferin, and metastasis was monitored by bioluminescence imaging with an IVIS Lumina II imaging system (PerkinElmer, Hopkinton, MA, USA). All animal experiments were approved by the Ethics Committee for Animal Experiments of Guangzhou Medical University.

2.24. Statistical analysis

All *in vitro* experiments were repeated three times independently. Statistical analyses were performed by using GraphPad Prism 7.0 (GraphPad Software Inc., La Jolla, CA, USA). All quantitative data are presented as the means ± SDs and were compared by a *t*-test. *P* values < 0.05 were considered to indicate significance in all experiments.

3. Results

3.1. High KCTD4 expression is associated with poor prognosis in ESCC patients and promotes cancer metastasis

Metastasis is the main cause of death in ESCC, and lymph node metastasis is a key indicator of tumor cell spread and a strong predictor of poor survival in ESCC patients[23,24]. To identify the key drivers of ESCC metastasis, we compared the mRNA profiles of three pairs of primary tumors and matched lymph node metastatic tissues and found that 495 genes were significantly upregulated in metastatic tissues (fold change >3). Overlapping these genes with the 149 genes upregulated in highly metastatic cells compared with parental cells showed that 7 genes were common between the two sets of genes. In particular, KCTD4 was chosen for further research because of its unknown function in the progression of cancer, and its apparent effect in promoting invasion compared with other candidate genes (Fig. 1A, Supporting Information Fig. S1A). The gene expression discrimination between primary tumors and matched lymph node metastatic tissues were displayed in a heatmap visualization (Fig. 1B). To determine the clinical relevance of KCTD4 in ESCC, a TMA consisting of 180 primary tumors and 158 matched normal tissues was employed, and we noted that KCTD4 expression was significantly higher in tumor tissues than in normal tissues (Fig. 1C). Moreover, high KCTD4 expression was closely associated with lymph node metastasis in cancer patients (Table 1). The patients with high KCTD4 expression had a shorter survival time (13.0 months) than the patients with low KCTD4 expression (37.0 months) (Fig. 1D). Analysis of KCTD4 expression in a TMA containing 40 pairs of primary tumor tissues and metastatic tissues indicated that KCTD4 was significantly upregulated in metastatic tissues compared with primary tumor tissues (Fig. 1E).

To investigate the biological function of KCTD4 in cancer metastasis, KCTD4 was ectopically overexpressed in KYSE150 and KYSE410 cells, and KYSE150-Luc-LM3 and KYSE270 cell lines with high KCTD4 expression were used to establish KCTD4-knockdown cells (Fig. S1B). Increased fibronectin expression and decreased E-cadherin expression were observed in KCTD4-overexpressing cells compared with the vector control cells (Fig. 1F). The results of the Boyden chamber assay demonstrated that the number of invading KCTD4-overexpressing cells was strikingly increased (Fig. 1G). In addition, a footpad inoculation model was established, and KCTD4-overexpressing cells were found to have a greater potential to metastasize to swollen popliteal lymph nodes (Fig. 1H). We obtained consistent results in the lung metastasis mouse model (Fig. 1I). The role of KCTD4 in cancer was confirmed by loss-of-function experiments showing that knockout of KCTD4 markedly suppressed ESCC cell invasion, lymph node metastasis, and lung metastasis (Fig. 1J−L).

(D) Kaplan−Meier analysis of overall survival for 180 ESCC patients stratified by the KCTD4 level. (E) Distribution of KCTD4 in 40 paired primary ESCC and matched metastatic tissues. (F) The expression of Fibronectin and E-cadherin was measured when KCTD4 was overexpressed. (G) Invasion assay showing the increased cell invasion upon KCTD4 overexpression. (H) Representative images and quantification of swollen inguinal lymph node metastases in mice injected with KCTD4-overexpressing or vector cells (n = 6). (I) Bioluminescence imaging and quantification of lung metastasis in mice injected intravenously with KCTD4-overexpressing or vector cells (n = 6). (J) Fibronectin and E-cadherin expression was evaluated when KCTD4 expression was inhibited *via* shRNA. (K) Quantification of cell invasion when KCTD4 was knocked down. (L) Bioluminescence images and quantification of swollen inguinal lymph node metastasis in mice injected with KCTD4-knockdown and vector control cells (n = 6). (M) Representative images and quantification of lung metastasis in mice injected with KCTD4-knockdown cells and control vector cells (n = 6). Bars, SDs; n.s.: not significant; *$P < 0.05$; **$P < 0.01$; ***$P < 0.001$.
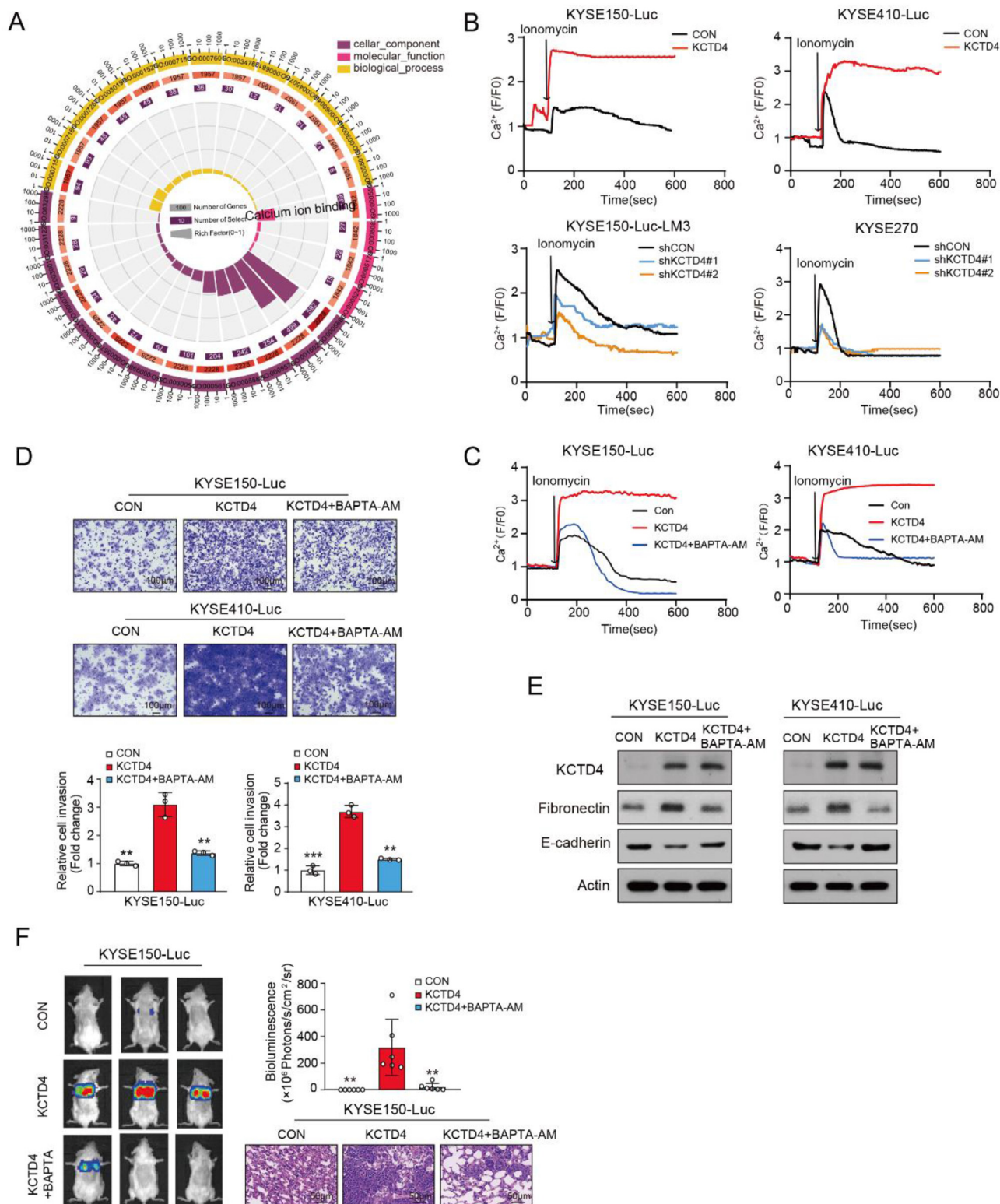
Figure 2 Ca^{2+} signaling mediates the effect of KCTD4 on cancer metastasis. (A) Gene Ontology Analysis (GO) indicating the activation of Ca^{2+} signaling in KCTD4-overexpressing cells. (B) By stimulation with ionomycin (10 μmol/L), calcium flux was analyzed in ESCC cells with modulation of KCTD4 expression. (C) Calcium flux was analyzed in the KCTD4-overexpressing cells in the presence or absence of BAPTA-AM (10 μmol/L). (D) The invasive potential of KCTD4-overexpressing cells was evaluated in the presence and absence of BAPTA-AM. (E) KCTD4, fibronectin and E-cadherin expression was evaluated in KCTD4-overexpressing cells in the presence and absence of BAPTA-AM. (F) Representative images and quantification of lung metastasis of KCTD4-overexpressing cells with or without BAPTA-AM (5 mg/kg, twice a week) treatment ($n = 6$). Bars, SDs; n. s.: not significant; $*P < 0.05$; $**P < 0.01$; $***P < 0.001$.
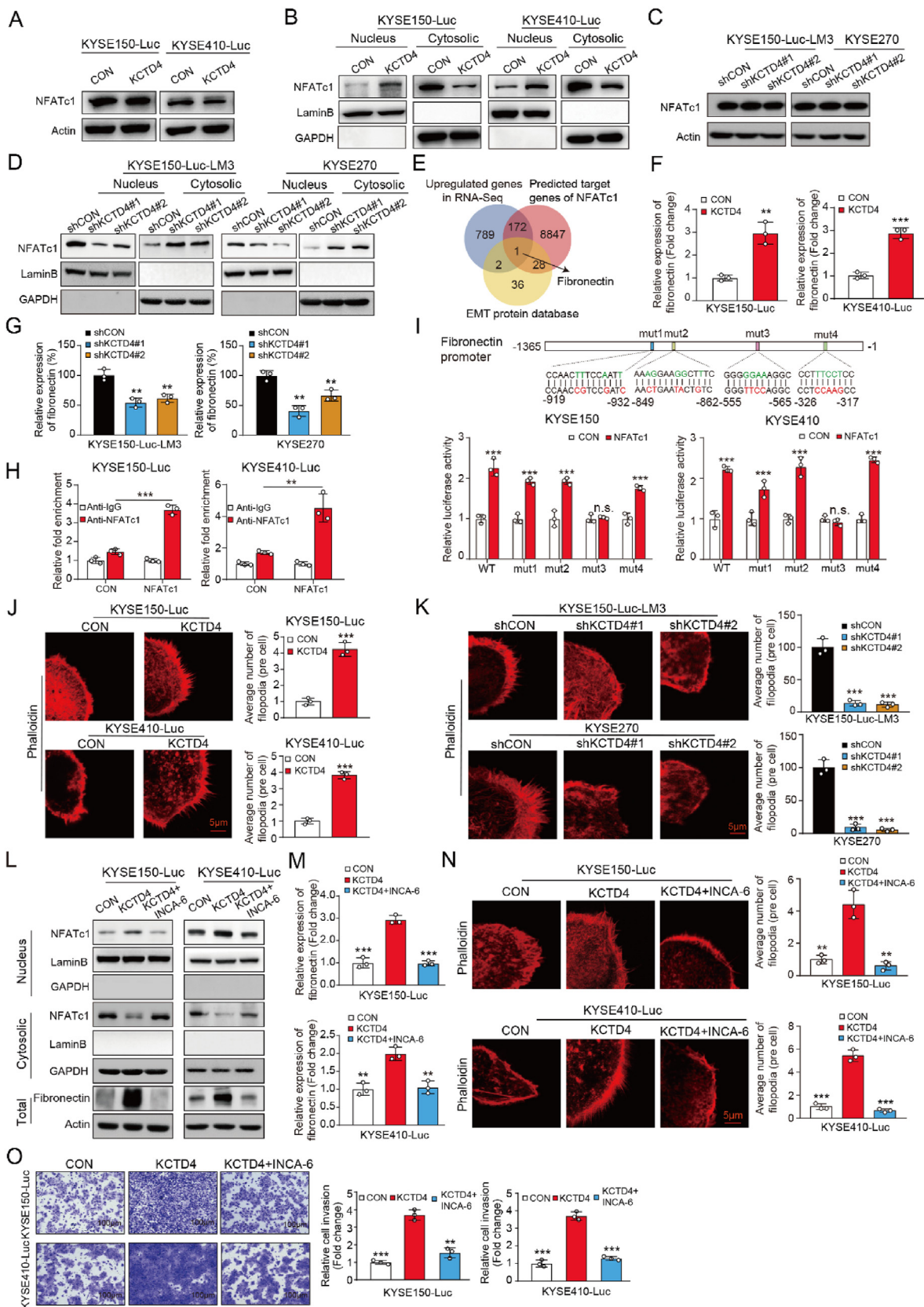
Figure 3　KCTD4 regulates ESCC metastasis *via* the Ca^{2+}-NFATc1-fibronectin axis. (A) Western blot analysis showing the expression of NFATc1 when KCTD4 was overexpressed. (B) Nuclear and cytoplasmic distribution of NFATc1 when KCTD4 was overexpressed. (C) Expression of NFATc1 when KCTD4 was knocked down *via* shRNA. (D) Cellular localization of NFATc1 when KCTD4 was knocked down. (E) Venn diagram showing the approach used to study the downstream genes of interest. (F−G) The RNA level of fibronectin after modulation of KCTD4

Collectively, these data imply the clinical and functional significance of KCTD4 in ESCC metastasis.

3.2. KCTD4 increases intracellular Ca^{2+} flux to promote cancer metastasis

To explore the molecular mechanisms underlying the role of KCTD4 in ESCC metastasis, RNA-seq was performed to compare the gene profiles between KCTD4-overexpressing cells and control cells. GO analysis of the differentially expressed genes suggested that Ca^{2+} signaling may be involved in the mechanism of action of KCTD4 (Fig. 2A). A Fluro-4 AM probe was adopted to monitor Ca^{2+} flux in ESCC cells, and the results showed that overexpression of KCTD4 increased and KCTD4 knockdown decreased intracellular Ca^{2+} levels (Fig. 2B, Supporting Information Fig. S2). To investigate the importance of Ca^{2+} in KCTD4-induced cancer cell invasion and metastasis, in vitro and in vivo assays were performed in the presence and absence of BAPTA-AM, an intracellular Ca^{2+} chelator (Fig. 2C). The invasion and metastasis induced by KCTD4 overexpression were significantly attenuated by BAPTA-AM, suggesting that KCTD4 promotes ESCC metastasis in a Ca^{2+}-dependent manner (Fig. 2D−F).

3.3. Ca^{2+}-induced NFATc1-fibronectin signaling mediates the role of KCTD4 in cancer metastasis

NFATc1 has been reported to translocate into the nucleus upon Ca^{2+} stimulation and regulate the expression of downstream genes as a transcription factor[25,26]. We studied the effect of KCTD4 on NFATc1. Overexpression of KCTD4 had no effect on the total expression but significantly induced the nuclear translocation of NFATc1 (Fig. 3A−B, Supporting Information Fig. S3A). In contrast, lower nuclear NFATc1 expression was observed in KCTD4-knockdown cells (Fig. 3C−D, Fig. S3B). To explore the downstream effectors through which Ca^{2+}-NFATc1 enhances cancer invasion, we compared the following three gene sets: 1) predicted downstream genes of NFATc1 obtained from the Harmonizome database (https://maayanlab.cloud/Harmonizome/), 2) genes upregulated upon KCTD4 overexpression as identified by RNA-seq, and 3) EMT-related genes obtained from published databases[27]. Interestingly, fibronectin was the only gene found to be common to all three sets and thus attracted our attention (Fig. 3E). We observed positive regulation of fibronectin mRNA expression by manipulation of KCTD4 expression (Fig. 3F−G). To investigate whether NFATc1 acts as a transcription factor to activate fibronectin expression, ChIP assay was performed to verify the binding of NFATc1 to the fibronectin promoter (Fig. 3H). The results of the dual luciferase reporter assay indicated that NFATc1 significantly enhanced the transcriptional activity of the fibronectin promoter and that this effect was remarkably abolished when the NFATc1 binding sites in the fibronectin promoter were mutated (Fig. 3I). Moreover,

immunofluorescence staining showed that overexpression of KCTD4 induced but knockdown of KCTD4 inhibited the formation of filopodia (Fig. 3J−K). Furthermore, INCA-6, a calcineurin−NFAT interaction inhibitor, was applied to determine whether the NFATc1 pathway is involved in the biological function of KCTD4. INCA-6 not only attenuated the mRNA and protein expression of fibronectin but also abolished filopodia formation and cell invasion induced by KCTD4 (Fig. 3L−O, Fig. S3C). In addition, knockdown of NFATc1 significantly reduced the invasive ability of KCTD4-overexpressing ESCC cells (Fig. S3D−E), supporting that NFATc1 is required for the KCTD4-induced metastasis. These data collectively demonstrate that Ca^{2+}-NFATc1 signaling is important for the function of KCTD4 in regulating cancer metastasis.

3.4. KCTD4-overexpressing cancer cells secrete fibronectin to activate fibroblasts in a paracrine manner

Considering the important role of fibronectin in cell−cell cross-talk[28,29], we speculated that KCTD4-overexpressing ESCC cells may induce the secretion of fibronectin to reprogram the TME in a paracrine manner. The ELISA and Western blot results confirmed that the level of secreted fibronectin in the CM from KCTD4-overexpressing ESCC cells (CM^{KCTD4}) was significantly higher than that in the CM from control cells (CM^{CON}) (Fig. 4A−B). In addition, CM^{KCTD4} not only enhanced the migration of fibroblasts (Fig. 4C−D) but also increased the expression levels of the myofibroblast markers α-smooth muscle actin (α-SMA) and fibroblast activation protein (FAP), suggesting that fibroblasts were activated by CM^{KCTD4} (Fig. 4E). Notably, this effect was abolished when an anti-fibronectin neutralizing antibody was added to the cancer cell-derived CM (Fig. 4F), indicating the important role of fibronectin in the paracrine effect of KCTD4-overexpressing cancer cells on fibroblasts.

We next examined whether activated fibroblasts exert a feedback effect on cancer cells. To this end, a coculture system was established using fibroblasts and KCTD4-overexpressing ESCC cells or control cells (Fig. 4G). The invasive ability of ESCC cells was markedly enhanced by CM from fibroblasts cocultured with KCTD4-overexpressing cancer cells compared with CM from fibroblasts cocultured with control cells (Fig. 4H). To elucidate the underlying mechanisms, an antibody microarray detecting 507 cytokines was used to compare the secretome in the CM from fibroblasts cocultured with KCTD4-overexpressing cancer cells with that in the CM from control cells. Among the top 10 upregulated cytokines, MMP24, FGF-19, PIGF and APRIL 4 were chosen for further study because they have been recognized to exert an oncogenic effect on cancer cells (Fig. 4I). Data from ELISA of the fibroblast-derived CM confirmed that secretion of MMP24 but not the others cytokines was positively regulated by ectopic expression of KCTD4 in cancer cells (Fig. 4J−K). Furthermore, knockdown of MMP24 in fibroblasts significantly attenuated the paracrine effect of activated fibroblasts on the

---

expression was determined by PCR. (H) A ChIP assay was performed to verify the binding of NFATc1 to the fibronectin promoter. (I) Diagram showing the design of mutants and the results of dual luciferase reporter assays showing that NFATc1 significantly enhanced the transcriptional activity of the wild-type fibronectin promoter but not its mutants. (J−K) Immunofluorescence staining showing the formation of filopodia in KCTD4-overexpressing and KCTD4-knockdown cells. (L−M) RNA and protein levels of fibronectin in KCTD4-overexpressing cells upon treatment with INCA-6. (N) Representative images showing that the formation of filopodia induced by overexpression of KCTD4 was attenuated by treatment with INCA6. (O) The invasion of KCTD4-overexpressing cells was evaluated in the presence of INCA-6 (10 μmol/L). Bars, SDs; n.s.: not significant; *$P < 0.05$; **$P < 0.01$; ***$P < 0.001$.
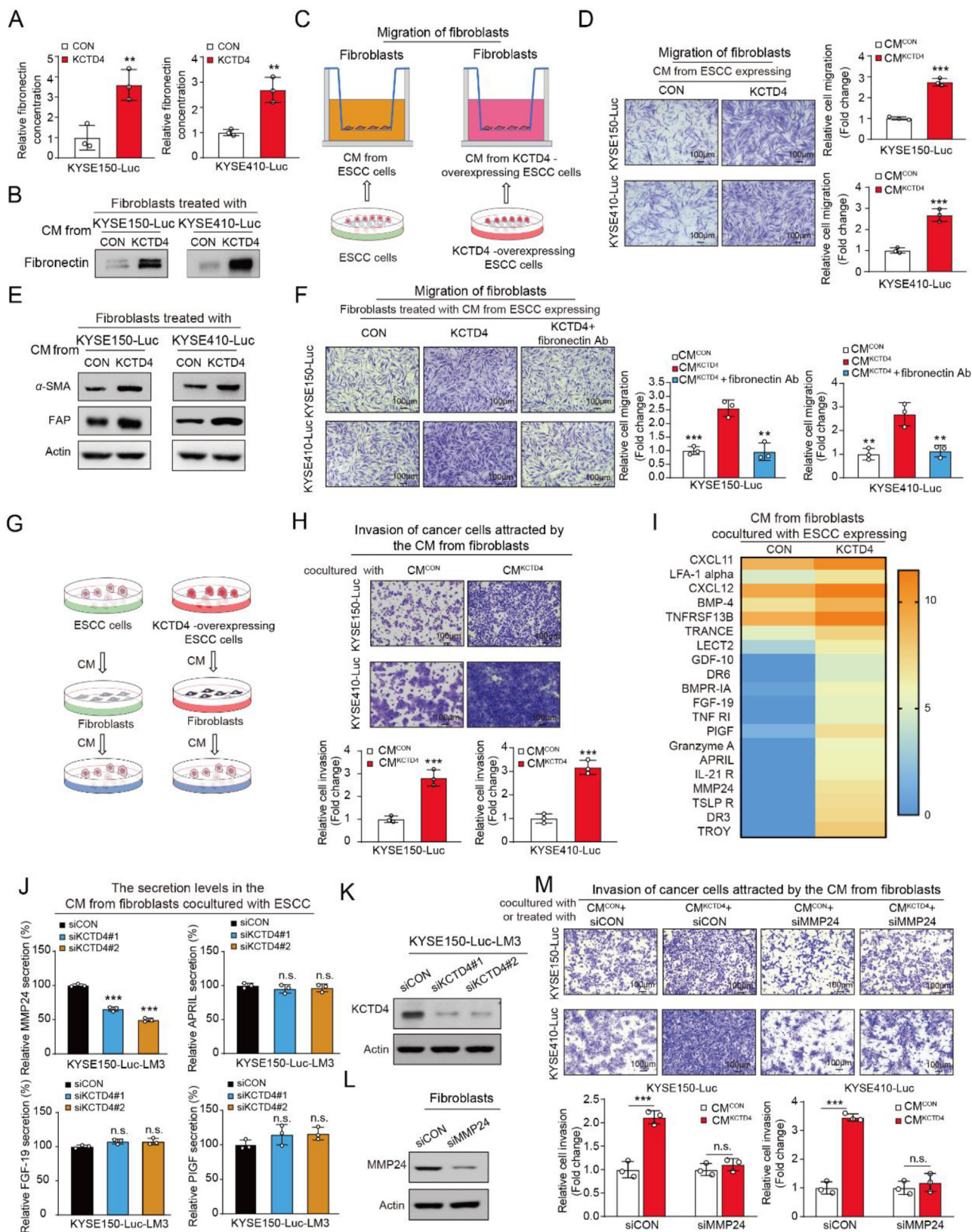
Figure 4 KCTD4-overexpressing tumor cells induce fibronectin secretion and fibroblast activation. (A) The level of secreted fibronectin in the CM of ESCC cells was quantified with an ELISA kit. (B) Western blot analysis showing the level of fibronectin in the CM from KCTD4-overexpressing and control ESCC cells. (C–D) Diagram and quantification of the collection of CM from the indicated ESCC cells to attract migrating fibroblasts. (E) The expression of α-SMA and FAP in fibroblasts was determined by Western blot analysis. (F) Blockade of fibronectin with a neutralizing antibody decreased the KCTD4 overexpression-induced migration of fibroblasts. (G) Diagram showing the approach for

invasive ability of ESCC cells (Fig. 4L−M). These data collectively suggest that fibronectin and MMP24 are essential for the crosstalk between cancer cells and fibroblasts in ESCC.

3.5. KCTD4 interacts with CLIC1 to disrupt its dimerization

To show the molecular mechanisms by which KCTD4 activates Ca^{2+}-NFATc1 signaling, IP-MS was performed to identify the binding partners of KCTD4. Among the interacting proteins, CLIC1, a member of the chloride channel protein family, attracted our attention because inhibition of its function can increase intracellular Ca^{2+} levels via L-type Ca^{2+} channels (LTCCs) (Fig. 5A)[30]. First, the interaction of KCTD4 and CLIC1 was confirmed by Co-IP assay (Fig. 5B). Second, a series of amino acids in the KCTD4 and CLIC1 proteins, including LYS17, ASP72, and ASP74 in KCTD4 and GLU102, LYS138, and ARG208 in CLIC1, were predicted by molecular docking to be responsible for the KCTD4−CLIC1 interaction (Fig. 5C). By performing site-directed mutagenesis, LYS17, ASP72, and ASP74 in KCTD4 were mutated and designated as KCTD4^{Mut}, whereas GLU102, LYS138, and ARG208 in CLIC1 were mutated and designated as CLIC1^{Mut}. The immunoprecipitation data showed that KCTD4 failed to bind to CLIC1 when these key sites were mutated (Fig. 5D−E).

Since CLIC1 needs to form dimers from its monomers to perform its chloride channel function[31], we postulated that KCTD4 may competitively bind to CLIC1 to block the formation of CLIC1 dimers, thereby inducing LTCC activity. To test the effect of KCTD4 on CLIC1 dimerization, ESCC cells with or without KCTD4 overexpression were co-transfected with CLIC1-HA or CLIC1-His. Our IP results showed that KCTD4 disrupted the dimerization of CLIC1 (Fig. 5F), which was further confirmed by native PAGE (Fig. 5G). We next examined whether the interaction between KCTD4 and CLIC1 affects the intracellular Cl^- level, and the MQAE assay data indicated that overexpression of KCTD4 led to an increased intracellular Cl^- level (Fig. 5H). Since an increase in Cl^- has been reported to increase intracellular Ca^{2+} via the activation of Ca^{2+} channels[32], we next studied whether LTCCs participate in the biological function of KCTD4. A series of in vitro and in vivo functional assays demonstrated that amlodipine, an LTCC blocker, not only abolished the effects of KCTD4 on the nuclear translocation of NFATc1 and the expression of fibronectin (Fig. 5I−K, Supporting Information Fig. S4) but also attenuated KCTD4-induced filopodia formation (Fig. 5L) and cancer cell invasion and metastasis (Fig. 5M−N).

3.6. CLIC1 is essential for the biological function of KCTD4 in cancer

To investigate the importance of CLIC1 in the biological function of KCTD4, the CRISPR/Cas9 system was used to establish CLIC1-knockout (CLIC1-KO) cells (Fig. 6A), and KCTD4 was further overexpressed in these cells, which were then subjected to functional experiments. Overexpression of KCTD4 failed to affect

the intracellular Ca^{2+} level, subcellular distribution of NFATc1 or formation of filopodia in CLIC1-deficient cells (Fig. 6B−D). More importantly, unlike in CLIC1-expressing cells, no change in the invasive or metastatic potential was observed in CLIC1-deficient ESCC cells upon overexpression of KCTD4 (Fig. 6E−F). Collectively, these results show that KCTD4 contributes to cancer metastasis in a CLIC1-dependent manner.

3.7. Identification of the lead compound K279-0738 as an inhibitor of the KCTD4−CLIC1 interaction to suppress cancer metastasis

Given the important role of the KCTD4−CLIC1 complex in cancer metastasis, blockade of this interaction might be an effective antimetastatic strategy. The binding sites of KCTD4 and CLIC1 were used as active cavities for molecular docking to screen for inhibitors that could block the interaction of KCTD4 and CLIC1. According to Lipinski's Rule of Five, the top 30 small molecules were selected for further research (Fig. 7A, Supporting Information Table S4). A modified ELISA (Super-ELISA), which was used in our previous study to screen for small molecules targeting protein−protein interactions[22], and Co-IP were performed to narrow down the list of candidate compounds targeting the KCTD4−CLIC1 interaction (Fig. 7B−C). Furthermore, by integration of the results from the chamber invasion assay, the small molecule #9 (K279-0738) was proposed as the compound of interest for further investigation (Fig. 7D, Supporting Information Fig. S5A). Compared to the small molecule #8 (K279-1502) as a control, K279-0738 not only reduced intracellular Ca^{2+} level and the nuclear translocation of NFATc1 (Fig. 7E−G, Fig. S5B−D), but also decreased fibronectin expression and the formation of filopodia in ESCC cells (Fig. 7H−J, Fig. S5E−G). The results from the Boyden chamber assay demonstrated that K279-0738 suppressed the invasion of ESCC cells in a dose-dependent manner (Fig. 7K, Fig. S5H). In addition, K279-0738 also suppressed the MMP24 level in fibroblasts (Fig. S5I). All the data demonstrated that K279-0738 is an inhibitor of the KCTD4−CLIC1 interaction to suppress cancer metastasis (Supporting Information Fig. S6A−C). In addition, the results from CCK8 and colony formation assays showed that K279-0738 had no effect on cell proliferation (Fig. S6D−E). To further examine the therapeutic potential of K279-0738 in a preclinical setting, we established an experimental lung metastasis model, and the results indicated that treatment with K279-0738 exerted a significant inhibitory effect on tumor metastasis (Fig. 7L). The toxicity of K279-0738 was evaluated by monitoring the histology of critical organs, and we did not note significant changes in the livers, spleen or kidneys of mice (Fig. S6F).

4. Discussion

ESCC is a serious malignancy and the sixth leading cause of cancer-related death[33,34]. At the time of diagnosis, most tumors have already invaded the lymph nodes or distant organs[35].

---

collecting CM from fibroblasts to study the feedback effect of fibroblasts on ESCC cells. (H) Invasion assay showing the invasive ability of ESCC cells attracted by CM from different fibroblast lines as indicated. (I) A cytokine chip was used to obtain the cytokine profiles of the groups, and the genes of interest and expression fold changes are presented in a heatmap. (J) The level of MMP24 in the CM from the indicated fibroblasts was quantified by an ELISA kit. (K) KCTD4 expression was evaluated in ESCC cells when KCTD4 was inhibited via siRNA. (L) MMP24 expression was evaluated in fibroblasts when MMP24 was inhibited via siRNA. (M) Quantitative analysis showing that knockdown of MMP24 in fibroblasts via siRNA decreased the invasion of KCTD4-overexpressing ESCC cells. Bars, SDs; n.s.: not significant; *$P < 0.05$; **$P < 0.01$; ***$P < 0.001$.
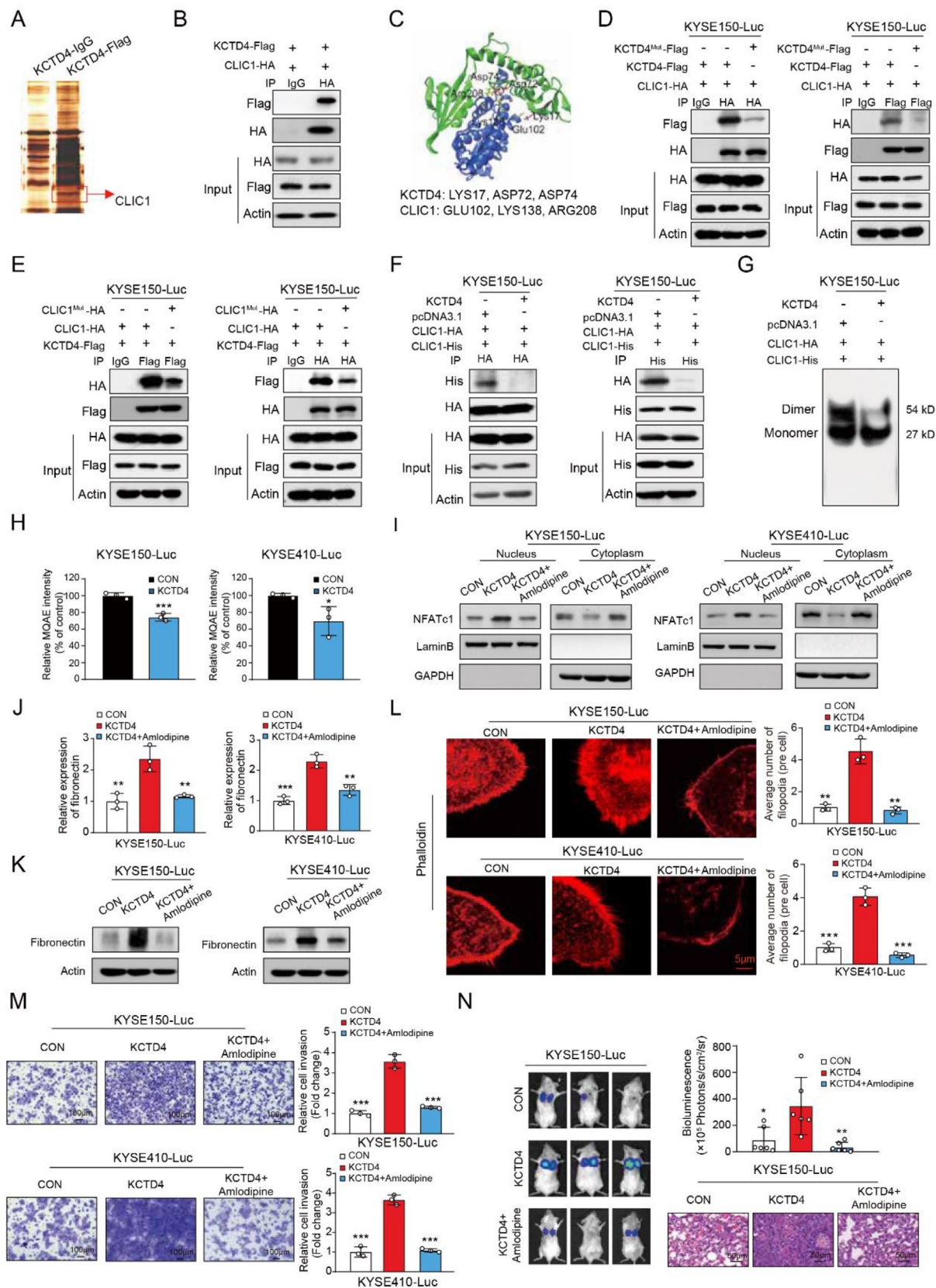
Figure 5 KCTD4 activates LTCCs by inhibiting CLIC1 dimerization. (A) Identification of KCTD4-interacting proteins by IP-MS. (B) Immunoprecipitation and Western blot results showing the interaction of KCTD4 and CLIC1. (C) Molecular docking showing the binding between KCTD4 and CLIC1. (D) ESCC cells were transfected with wild-type KCTD4 or mutant expression plasmids, and the interaction of KCTD4 with CLIC1 was evaluated by immunoprecipitation and Western blotting. (E) Mutation of CLIC1 abolished its interaction with KCTD4. (F)
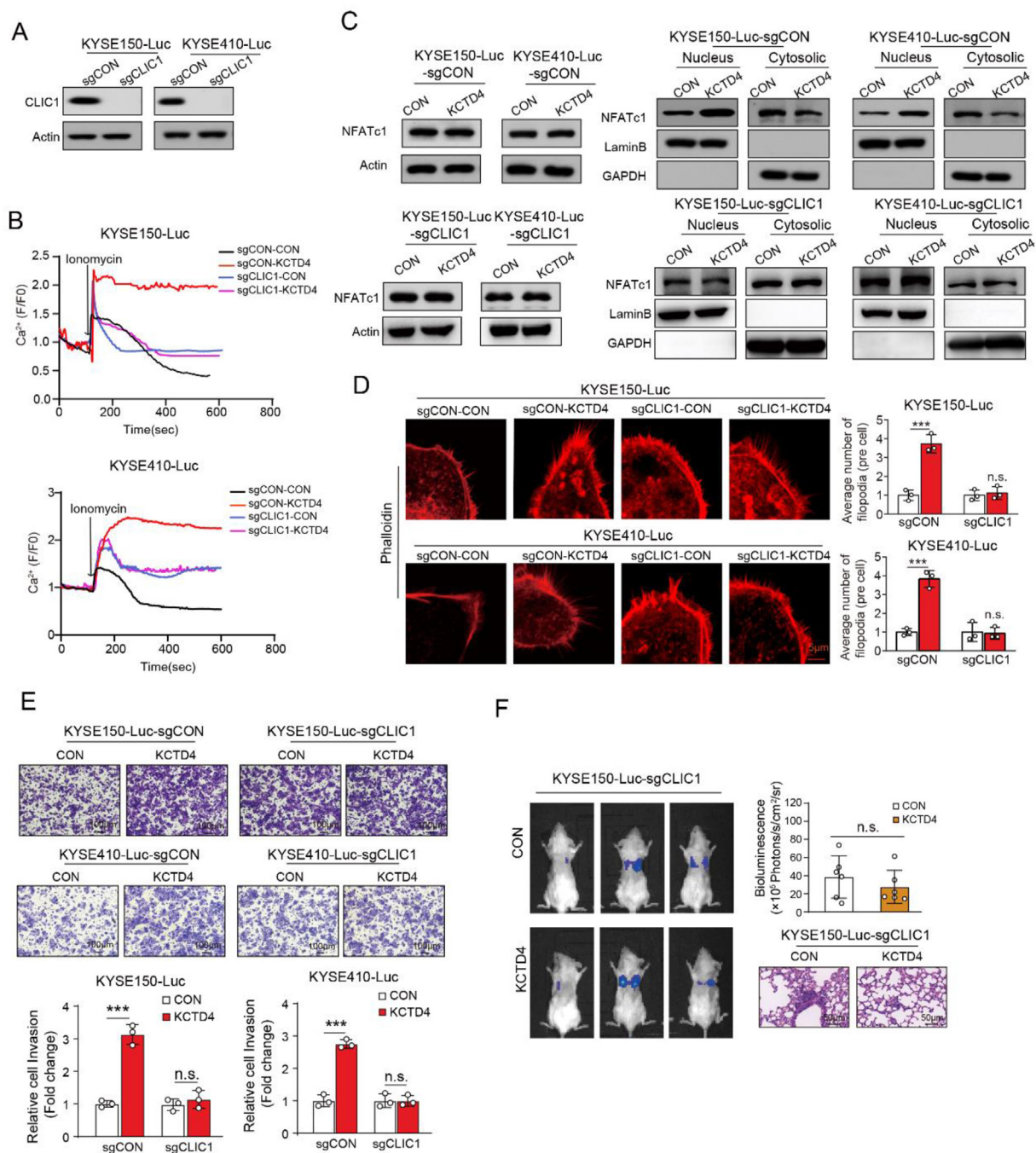
Figure 6 KCTD4 promotes cancer metastasis by interacting with CLIC1. (A) Successful knockout of CLIC1 in KYSE150-Luc and KYSE410-Luc cells. (B) Calcium flux data showing that CLIC1 knockout reduced the intracellular Ca^{2+} flux in KCTD4-overexpressing cells. (C–D) Effects of CLIC1 knockout on NFATc1 expression, NFATc1 distribution and formation of pseudopodia. (E) CLIC1-KO cells were subjected to further overexpression of the KCTD4 or control plasmid, and cell invasion was evaluated. (F) CLIC1-KO cells were subjected to further overexpression of KCTD4, and metastasis was investigated ($n = 6$). Bars, SDs; n.s.: not significant; *$P < 0.05$; **$P < 0.01$; ***$P < 0.001$.

Immunoprecipitation results showing that KCTD4 inhibits the interaction of CLIC1-HA and CLIC1-His. (G) KCTD4 inhibited the formation of CLIC1 dimers, as shown by native PAGE. (H) MQAE intensity data showing that KCTD4 regulates intracellular chloride ion levels. (I) Western blot analysis showing that the LTCC inhibitor amlodipine inhibited the nuclear accumulation of NFATc1. (J–K) Amlodipine abolished the effect of KCTD4 on the RNA and protein expression of fibronectin. (L) The formation of pseudopodia was visualized by immunofluorescence staining in the presence and absence of amlodipine. (M) Invasion assay showing that treatment with amlodipine (10 μmol/L) inhibited KCTD4-induced invasion. (N) Bioluminescence imaging and quantification of lung metastasis showing metastasis in mice treated with or without amlodipine (10 mg/kg, twice a week) ($n = 6$). Bars, SDs; n.s.: not significant; *$P < 0.05$; **$P < 0.01$; ***$P < 0.001$.
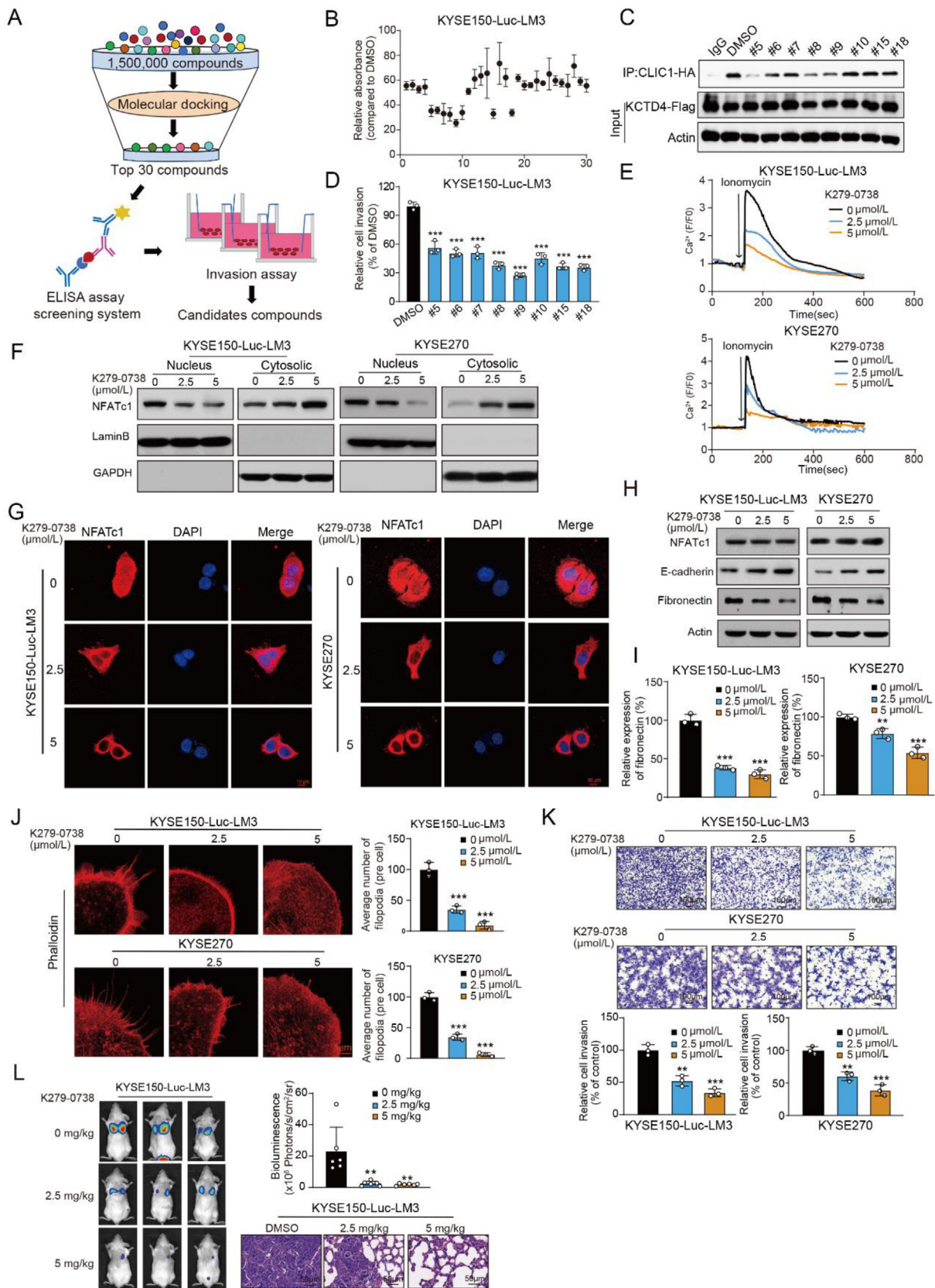
Figure 7   Identification of K279-0738 as a disruptor of the KCTD4−CLIC1 interaction and cancer metastasis. (A) Diagram showing the strategy used to screen the candidate compounds. (B) An ELISA screening system was used to screen for potential inhibitors of the interaction between the recombinant KCTD4 protein and CLIC1. (C) IP assay showing the binding of KCTD4 and CLIC1 in the presence of the inhibitors as indicated. (D) Comparison of invasion among cells treated with the 8 candidate compounds. (E) K279-0738 reduced the intracellular Ca^{2+} flux.
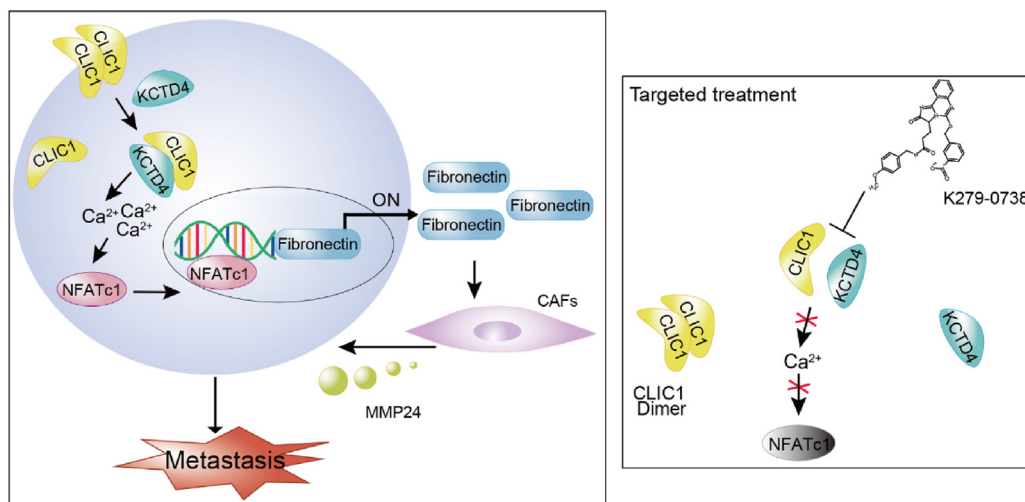
Figure 8   Schematic diagram summarizing how KCTD4 promotes cancer metastasis.

Therefore, the identification of effective chemotherapeutic and targeted drugs is an urgent need for ESCC therapy. Fibronectin is a high-molecular-weight glycoprotein found in the extracellular matrix (ECM) that has been reported to play diverse biological roles in cellular development, differentiation, adhesion and migration, mainly through integrin-mediated signaling[36]. The binding of fibronectin to integrins induces receptor clustering and brings cytoplasmic molecules together to generate focal complexes that activate actin filament polymerization[37]. To date, most studies have focused on the downstream effectors of fibronectin, and the upstream regulators of fibronectin remain largely unclear. Here, we provide the first evidence that KCTD4-induced Ca^{2+} influx promotes NFATc1 nuclear localization to activate fibronectin transcription, identifying KCTD4-Ca^{2+}-NFATc1 signaling as a novel upstream mechanism of fibronectin expression.

The TME is a complex network consisting of many kinds of stromal cells, such as CAFs, and ECM[38]. Secreted fibronectin binds to ECM proteins, cell surface receptors, blood protein derivatives or glycosaminoglycans, participating in subsequent cellular processes[39]. A recent study demonstrated that fibronectin can act as a competence factor to promote the growth of fibroblasts[28]. However, the effect of fibronectin on the ESCC microenvironment and cancer metastasis remains largely unknown. Here, we demonstrated that the cancer cell-derived fibronectin, whose secretion is induced by KCTD4-Ca^{2+}-NFATc1 signaling, initiated the activation of fibroblasts in a paracrine manner, whereas a neutralizing antibody against fibronectin attenuated this effect. In addition, by performing a cytokine antibody microarray screen and subsequent functional rescue experiments, we showed that fibronectin-activated fibroblasts can secrete MMP24 to promote ESCC cell invasion as positive feedback. It is worth noting that in addition to fibroblasts, there are many other stromal cells in

the TME, and the effects of KCTD4-induced fibronectin on other cellular components warrants further study.

Chloride is a major anion and electrolyte that contributes to the osmotic pressure across the plasma membrane. CLIC1 is a non-canonical self-assembling anion channel and participates in multiple cellular functions, including apoptosis and tumorigenesis[40]. A homologous protein in the GST superfamily, CLIC1 is assembled in a multimeric conformation from its soluble cytosolic form and inserted into cell membranes to form chloride ion channels[40], which can also regulate cellular Ca^{2+} and its associated signaling pathways. In this study, we not only demonstrated that the interaction of KCTD4 with CLIC1 affects the formation of CLIC1 dimers, thereby causing an increase in intracellular Ca^{2+} *via* LTCCs, but also proposed that the metastasis-driving effect of KCTD4 is CLCL1 dependent. To our knowledge, this is the first study to delineate the function of the KCTD4−CLIC1 complex in the regulation of Ca^{2+} homeostasis and cancer.

Disruption of the KCTD4−CLIC1 interaction might be a promising strategy to suppress tumor metastasis. In the present study, we aimed to develop inhibitors that satisfied three criteria: 1) inhibit the interaction between KCTD4 and CLIC1; 2) suppress ESCC cell invasion and metastasis; and 3) exert no obvious side effects. Integration of the results of *in silico* predictions, Super ELISA and the high-throughput invasion assay revealed that K279-0738 is a potential lead compound targeting the KCTD4−CLIC1 interaction to suppress cancer metastasis. On the one hand, molecular design and further optimization of the K279-0738 structure may facilitate its clinical application in cancer treatment; on the other hand, the therapeutic efficacy of the combination of K279-0738 with immunotherapeutic agents warrants further exploration.

Taken together, our findings reveal KCTD4 as a novel driver of ESCC metastasis. Mechanistically, KCTD4 inhibits CLIC1

(F−G) Effect of K279-0738 on the nuclear accumulation of NFATc1. (H) The protein expression of E-cadherin and fibronectin in K279-0738-treated ESCC cells. (I) The mRNA expression of fibronectin in K279-0738-treated ESCC cells. (J) Effect of K279-0738 on formation of filopodia. (K) Invasion assay showing that K279-0738 inhibited ESCC cell invasion in a dose-dependent manner. (L) Bioluminescence imaging and quantification of lung metastasis showing that K279-0738 (twice a week) inhibited ESCC cell metastasis ($n = 6$). Bars, SDs; n.s.: not significant; *$P < 0.05$; **$P < 0.01$; ***$P < 0.001$.

dimerization to induce LTCC activity, subsequently activating the Ca^{2+}-NFATc1-fibronectin axis to activate fibroblasts, which promote cancer invasion in a paracrine manner (Fig. 8). Pharmacological inhibition of the KCTD4−CLCLI interaction provides useful insights for the development of therapeutic strategies for this lethal disease.

Acknowledgments

Author contributions

Cancan Zheng, Xiao-mei Yu, Taoyang Xu: acquisition of data; analysis and interpretation of data; statistical analysis; Zhichao Liu, Zhili Jiang, Jiaojiao Xu, Jing Yang, Guogeng Zhang, Yan He: acquisition of data, analysis and interpretation of data; Han Yang, Xingyuan Shi, Zhigang Li, Jinbao Liu: technical and/or material support and critical revision of the manuscript for important intellectual content; Wen Wen Xu: study concept and design; drafting of the manuscript; obtained funding; study supervision; All authors commented on the manuscript and approved the final manuscript.

Conflicts of interest

The authors declare no conflicts of interest.

Appendix A.   Supporting information

Supporting data to this article can be found online at https://doi.org/10.1016/j.apsb.2023.07.013.

References

1. Cao LJ, Zhang YJ, Dong SQ, Li XZ, Tong XT, Chen D, et al. ATAD2 interacts with C/EBPbeta to promote esophageal squamous cell carcinoma metastasis *via* TGF-beta1/smad3 signaling. *J Exp Clin Cancer Res* 2021;**40**:109.
2. Xu WW, Zheng CC, Zuo Q, Li JQ, Hong P, Qin YR, et al. Genome-wide identification of key regulatory lncRNAs in esophageal cancer metastasis. *Signal Transduct Targeted Ther* 2021;**6**:88.
3. Prevarskaya N, Skryma R, Shuba Y. Ion channels in cancer: are cancer hallmarks oncochannelopathies?. *Physiol Rev* 2018;**98**:559−621.
4. Ren R, Guo J, Chen Y, Zhang Y, Chen L, Xiong W. The role of Ca^{2+}/calcineurin/NFAT signalling pathway in osteoblastogenesis. *Cell Prolif* 2021;**54**:e13122.
5. Liu Z, Xiang Y, Sun G. The KCTD family of proteins: structure, function, disease relevance. *Cell Biosci* 2013;**3**:45.
6. Angrisani A, Di Fiore A, De Smaele E, Moretti M. The emerging role of the KCTD proteins in cancer. *Cell Commun Signal* 2021;**19**:56.
7. Littler DR, Harrop SJ, Fairlie WD, Brown LJ, Pankhurst GJ, Pankhurst S, et al. The intracellular chloride ion channel protein CLIC1 undergoes a redox-controlled structural transition. *J Biol Chem* 2004;**279**:9298−305.
8. Baghban R, Roshangar L, Jahanban-Esfahlan R, Seidi K, Ebrahimi-Kalan A, Jaymand M, et al. Tumor microenvironment complexity and therapeutic implications at a glance. *Cell Commun Signal* 2020; **18**:59.
9. Biffi G, Tuveson DA. Diversity and biology of cancer-associated fibroblasts. *Physiol Rev* 2021;**101**:147−76.
10. Kalluri R. The biology and function of fibroblasts in cancer. *Nat Rev Cancer* 2016;**16**:582−98.
11. Hu HF, Xu WW, Zhang WX, Yan X, Li YJ, Li B, et al. Identification of miR-515-3p and its targets, vimentin and MMP3, as a key regulatory mechanism in esophageal cancer metastasis: functional and clinical significance. *Signal Transduct Targeted Ther* 2020;**5**:271.
12. Yu XM, Li SJ, Yao ZT, Xu JJ, Zheng CC, Liu ZC, et al. N4-Acetylcytidine modification of lncRNA CTC-490G23.2 promotes cancer metastasis through interacting with PTBP1 to increase CD44 alternative splicing. *Oncogene* 2023;**42**:1101−16.
13. Xu WW, Li B, Guan XY, Chung SK, Wang Y, Yip YL, et al. Cancer cell-secreted IGF2 instigates fibroblasts and bone marrow-derived vascular progenitor cells to promote cancer progression. *Nat Commun* 2017;**8**:14399.
14. Liao L, He Y, Li SJ, Zhang GG, Yu W, Yang J, et al. Anti-HIV drug elvitegravir suppresses cancer metastasis *via* increased proteasomal degradation of m6A methyltransferase METTL3. *Cancer Res* 2022; **82**:2444−57.
15. Hong P, Liu QW, Xie Y, Zhang QH, Liao L, He QY, et al. Echinatin suppresses esophageal cancer tumor growth and invasion through inducing AKT/mTOR-dependent autophagy and apoptosis. *Cell Death Dis* 2020;**11**:524.
16. Zheng C, Zhu Y, Liu Q, Luo T, Xu W. Maprotiline suppresses cholesterol biosynthesis and hepatocellular carcinoma progression through direct targeting of CRABP1. *Front Pharmacol* 2021;**12**: 689767.
17. Deng CM, Zhang GG, Liu QW, Xu JJ, Liu ZC, Yang J, et al. ANO1 reprograms cholesterol metabolism and the tumor microenvironment to promote cancer metastasis. *Cancer Res* 2023;**83**:1851−65.
18. Tan XP, He Y, Huang YN, Zheng CC, Li JQ, Liu QW, et al. Lomerizine 2HCl inhibits cell proliferation and induces protective autophagy in colorectal cancer *via* the PI3K/Akt/mTOR signaling pathway. *MedComm* 2020;**2021**:453−66.
19. Zheng CC, Liao L, Liu YP, Yang YM, He Y, Zhang GG, et al. Blockade of nuclear beta-catenin signaling *via* direct targeting of RanBP3 with NU2058 induces cell senescence to suppress colorectal tumorigenesistumorigenesis. *Adv Sci* 2022;**9**:e2202528.
20. Zheng C, Yu X, Liang Y, Zhu Y, He Y, Liao L, et al. Targeting PFKL with penfluridol inhibits glycolysis and suppresses esophageal cancer tumorigenesis in an AMPK/FOXO3a/BIM-dependent manner. *Acta Pharm Sin B* 2022;**12**:1271−87.
21. Zuo Q, Liao L, Yao ZT, Liu YP, Wang DK, Li SJ, et al. Targeting PP2A with lomitapide suppresses colorectal tumorigenesis through the activation of AMPK/Beclin1-mediated autophagy. *Cancer Lett* 2021; **521**:281−93.
22. Yang J, Xu WW, Hong P, Ye F, Huang XH, Hu HF, et al. Adefovir dipivoxil sensitizes colon cancer cells to vemurafenib by disrupting the KCTD12−CDK1 interaction. *Cancer Lett* 2019;**451**:79−91.
23. Wang Y, Zhang W, Liu W, Huang L, Wang Y, Li D, et al. Long noncoding RNA VESTAR regulates lymphangiogenesis and lymph node metastasis of esophageal squamous cell carcinoma by enhancing VEGFC mRNA stability. *Cancer Res* 2021;**81**:3187−99.
24. Liao L, He Y, Li SJ, Yu XM, Liu ZC, Liang YY, et al. Lysine 2-hydroxyisobutyrylation of NAT10 promotes cancer metastasis in an ac4C-dependent manner. *Cell Res* 2023;**33**:355−71.
25. Son A, Kang N, Kang JY, Kim KW, Yang YM, Shin DM. TRPM3/TRPV4 regulates Ca^{2+}-mediated RANKL/NFATc1 expression in osteoblasts. *J Mol Endocrinol* 2018;**61**:207−18.

26. Kang JY, Kang N, Yang YM, Hong JH, Shin DM. The role of Ca^{2+}-NFATc1 signaling and its modulation on osteoclastogenesis. *Int J Mol Sci* 2020;**21**:3646.

27. Lin X, Chai G, Wu Y, Li J, Chen F, Liu J, et al. RNA m(6)A methylation regulates the epithelial mesenchymal transition of cancer cells and translation of Snail. *Nat Commun* 2019;**10**:2065.

28. Bitterman PB, Rennard SI, Adelberg S, Crystal RG. Role of fibronectin as a growth factor for fibroblasts. *J Cell Biol* 1983;**97**:1925−32.

29. Maheshwari G, Wells A, Griffith LG, Lauffenburger DA. Biophysical integration of effects of epidermal growth factor and fibronectin on fibroblast migration. *Biophys J* 1999;**76**:2814−23.

30. Lee JR, Lee JY, Kim HJ, Hahn MJ, Kang JS, Cho H. The inhibition of chloride intracellular channel 1 enhances Ca^{2+} and reactive oxygen species signaling in A549 human lung cancer cells. *Exp Mol Med* 2019;**51**:1−11.

31. Peter B, Polyansky AA, Fanucchi S, Dirr HW. A Lys-Trp cation−pi interaction mediates the dimerization and function of the chloride intracellular channel protein 1 transmembrane domain. *Biochemistry* 2014;**53**:57−67.

32. Saberbaghi T, Wong R, Rutka JT, Wang GL, Feng ZP, Sun HS. Role of Cl^- channels in primary brain tumour. *Cell Calcium* 2019;**81**:1−11.

33. Jia Y, Tian C, Wang H, Yu F, Lv W, Duan Y, et al. Long non-coding RNA NORAD/miR-224-3p/MTDH axis contributes to CDDP resistance of esophageal squamous cell carcinoma by promoting nuclear accumulation of beta-catenin. *Mol Cancer* 2021;**20**:162.

34. Yang YM, Hong P, Xu WW, He QY, Li B. Advances in targeted therapy for esophageal cancer. *Signal Transduct Targeted Ther* 2020;**5**:229.

35. Zhang J, Luo A, Huang F, Gong T, Liu Z. SERPINE2 promotes esophageal squamous cell carcinoma metastasis by activating BMP4. *Cancer Lett* 2020;**469**:390−8.

36. Yi M, Ruoslahti E. A fibronectin fragment inhibits tumor growth, angiogenesis, and metastasis. *Proc Natl Acad Sci U S A* 2001;**98**:620−4.

37. Spada S, Tocci A, Di Modugno F, Nistico P. Fibronectin as a multi-regulatory molecule crucial in tumor matrisome: from structural and functional features to clinical practice in oncology. *J Exp Clin Cancer Res* 2021;**40**:102.

38. Belli C, Trapani D, Viale G, D'Amico P, Duso BA, Della Vigna P, et al. Targeting the microenvironment in solid tumors. *Cancer Treat Rev* 2018;**65**:22−32.

39. Kaspar M, Zardi L, Neri D. Fibronectin as target for tumor therapy. *Int J Cancer* 2006;**118**:1331−9.

40. Barbieri F, Bosio AG, Pattarozzi A, Tonelli M, Bajetto A, Verduci I, et al. Chloride intracellular channel 1 activity is not required for glioblastoma development but its inhibition dictates glioma stem cell responsivity to novel biguanide derivatives. *J Exp Clin Cancer Res* 2022;**41**:53.